



Alteration of the late endocytic pathway in Charcot–Marie–Tooth type 2B disease

Roberta Romano¹ · Cristina Rivellini² · Maria De Luca¹ · Rossana Tonlorenzi² · Raffaella Beli¹ · Fiore Manganelli³ · Maria Nolano^{3,4} · Lucio Santoro³ · Eeva-Liisa Eskelinen^{5,6} · Stefano C. Previtali² · Cecilia Bucci¹

Received: 17 September 2019 / Revised: 18 March 2020 / Accepted: 24 March 2020 / Published online: 13 April 2020
© The Author(s) 2020

Abstract

The small GTPase RAB7A regulates late stages of the endocytic pathway and plays specific roles in neurons, controlling neurotrophins trafficking and signaling, neurite outgrowth and neuronal migration. Mutations in the *RAB7A* gene cause the autosomal dominant Charcot–Marie–Tooth type 2B (CMT2B) disease, an axonal peripheral neuropathy. As several neurodegenerative diseases are caused by alterations of endocytosis, we investigated whether CMT2B-causing mutations correlate with changes in this process. To this purpose, we studied the endocytic pathway in skin fibroblasts from healthy and CMT2B individuals. We found higher expression of late endocytic proteins in CMT2B cells compared to control cells, as well as higher activity of cathepsins and higher receptor degradation activity. Consistently, we observed an increased number of lysosomes, accompanied by higher lysosomal degradative activity in CMT2B cells. Furthermore, we found increased migration and increased RAC1 and MMP-2 activation in CMT2B compared to control cells. To validate these data, we obtained sensory neurons from patient and control iPS cells, to confirm increased lysosomal protein expression and lysosomal activity in CMT2B-derived neurons. Altogether, these results demonstrate that in CMT2B patient-derived cells, the endocytic degradative pathway is altered, suggesting that higher lysosomal activity contributes to neurodegeneration occurring in CMT2B.

Keywords RAB7A · Endocytosis · Lysosome · RAC1 · Migration · EGFR

Electronic supplementary material The online version of this article (<https://doi.org/10.1007/s00018-020-03510-1>) contains supplementary material, which is available to authorized users.

✉ Cecilia Bucci
cecilia.bucci@unisalento.it

¹ Department of Biological and Environmental Sciences and Technologies (DiSTeBA), University of Salento, Lecce, Italy

² Institute of Experimental Neurology (INSPE), IRCCS San Raffaele Scientific Institute, Milan, Italy

³ Department of Neurosciences, Reproductive Sciences and Odontostomatology, University of Naples “Federico II”, Naples, Italy

⁴ Salvatore Maugeri Foundation, Institute of Telesse Terme, Benevento, Italy

⁵ Institute of Biomedicine, University of Turku, Turku, Finland

⁶ Molecular and Integrative Biosciences Research Programme, University of Helsinki, Helsinki, Finland

Introduction

Endocytosis is an extremely regulated process by which cells internalize different plasma membrane components and molecules from the extracellular space [1]. This pathway plays a role in several cellular events, including termination of signaling pathways by targeting signaling receptors to degradation compartments such as late endosomes and lysosomes [1, 2]. Transport to late endosomes and lysosomes is finely controlled by sequential events and by several cellular proteins, including RAB GTPases, molecular motors and sorting regulators that altogether assure correct shipment to compartments [1, 3].

RAB7A, hereafter called RAB7, a ubiquitous RAB GTPase, regulates clustering and fusion of late endosomes and lysosomes in the perinuclear area, controlling biogenesis of and transport to lysosomes, phagolysosomes and autolysosomes [4–8]. Interestingly, several studies demonstrate that RAB7 plays specific roles in neurons, controlling axonal retrograde transport of neurotrophins, neurotrophin receptor signaling, neurite outgrowth and the final phase of immature

cortical neuron migration [9–14]. Furthermore, RAB7 interacts with and controls assembly of two intermediate filament proteins, peripherin and vimentin, which play an essential role in neurite outgrowth and axonal regeneration, and which also regulate the degradative endocytic pathway, providing positional information for late endocytic organelles and being responsible for their function [15–22].

Notably, a number of studies show that alterations of endocytic traffic and axonal transport are causative of several neurodegenerative diseases, such as Alzheimer's disease, Huntington's disease and amyotrophic lateral sclerosis [23]. In line with these findings, five missense mutations in the RAB7 gene cause Charcot–Marie–Tooth type 2B (CMT2B) disease, a rare inherited autosomal dominant neuropathy affecting the peripheral nervous system [24–27].

CMT2B is one of the numerous forms of CMT disease. It is an axonal neuropathy, characterized by progressive distal weakness and atrophy, accompanied by sensory loss and ulcero-mutilating complications [28–32]. CMT2B is a rare form of CMT and only one Italian family carrying the RAB7^{V162M} mutation has been identified up to now [33].

The biochemical properties of four CMT2B-causing mutants (RAB7^{L129F}, RAB7^{K157N}, RAB7^{N161T} and RAB7^{V162M}) have been previously investigated, demonstrating that these mutants show higher nucleotide K_{off} compared to the wild-type protein, and, therefore, release nucleotides faster [34–36]. As in the cell GTP concentration is higher than GDP, CMT2B mutants are mostly in the GTP-bound form, and were initially predicted to be active mutants [36]. However, these mutant proteins also release GTP faster than the wt protein, thus displaying a reduced GTPase activity per binding event [34–36], and, for this reason, they could inhibit activation of specific effectors while inducing activation of others. This hypothesis is corroborated by data in *Drosophila*, where neurodegeneration occurring in CMT2B is due to partial loss of function, and in zebrafish where axon growth and guidance defects are caused by a gain of function mechanism [37–39]. Therefore, CMT2B-causing mutations are neither "loss of function" nor "gain of function", but they behave as either inhibitory or activating, depending on kinetic requirements of the processes controlled by RAB7.

Importantly, the expression of CMT2B-causing RAB7 mutants alters several neuronal processes, modifying neurotrophin trafficking and, as a consequence, neurotrophin signaling pathways, thus resulting in inhibition of neurite outgrowth [40–42].

In this work, we analyzed different aspects of the endocytic pathway in skin fibroblasts and iPSC-derived sensory neurons. Interestingly, we found that patient-derived CMT2B cells display greater expression of lysosomal markers as well as higher lysosomal activity compared to control cells, suggesting that these alterations could contribute to neurodegeneration.

Materials and methods

Cells and reagents

Dermal fibroblasts derived from two healthy individuals (control fibroblasts) and from three CMT2B patients belonging to the same Italian family carrying the RAB7^{V162M} mutation were obtained as previously described [43]. After informed consent for pathological diagnosis, samples were anonymously encoded to protect patient confidentiality and used under protocols approved by the Azienda Ospedaliera Universitaria "Federico II" Ethics Committee (*Ethical Committee Approval Protocol # 107/05*). Fibroblasts were cultured in Dulbecco's modified Eagle's medium (DMEM) supplemented with 15% fetal bovine serum (FBS), 2 mM L-glutamine, 100 U/ml penicillin and 10 mg/ml streptomycin in a 5% CO₂ incubator at 37 °C. Chemicals and tissue culture reagents were from Sigma-Aldrich (St-Louis, MO, USA). HeLa cells were maintained in DMEM supplemented with 10% FBS, 2 mM L-glutamine, 100 U/ml penicillin and 10 mg/ml streptomycin in a 5% CO₂ incubator at 37 °C.

Antibodies

Primary antibodies used in this study were: mouse monoclonal anti-RAB7 (1:500, sc-376362), anti-RAB9 (1:200, sc-74482), anti-β-actin (1:1000, sc-47778), anti-RAC-GAP1 (1:200, sc-271110), anti-OCT3/4 (1:200; sc-5279) and anti EAP30 (1:200, sc-100892), rabbit polyclonal anti-RAB4 (1:200, sc-312), anti-RAB5 (1:200, sc-309), anti-ERK1 (1:200, sc-93), anti-HA (1:100, sc-805) and anti-pAKT (1:200, sc-7985-R), goat polyclonal anti-cathepsin D (1:500, sc-6486) from Santa Cruz Biotechnology, (Dallas, TX, USA); mouse monoclonal anti-tubulin (1:10,000, T5168) and anti-Smooth Muscle Actin (1:200; A2547) from Sigma-Aldrich (St. Louis, MO, USA); mouse monoclonal anti-cytokeratin CK8/18 (1:400; NCL-L-5D3) from Leica (Wetzlar, Germany); mouse monoclonal anti-LAMP2 (1:5000, H4B4), developed by J.T. August and J.E.K. Hildreth and obtained from the Developmental Studies Hybridoma Bank, (Iowa City, IA 52242); rabbit polyclonal anti-CI-MPR (1:2000, ab32815), anti-TSG101 (1:500, ab30871) anti-LAMP1 (1:4000, for immunoblot analysis and 1:1000 for immunofluorescence analysis, ab24170) and goat polyclonal anti-CGRP (1:200; ab36001) from Abcam (Cambridge, UK); rabbit polyclonal anti-peripherin (1:100, AB1530) and anti-Brn3a (1:100; AB5945) from Merck Millipore (Burlington, MS, USA); sheep polyclonal anti-TGN46 (1:500, AHP500) from Bio-Rad (Hercules, CA, USA); sheep polyclonal anti

EGFR (1:1000, 20-ES04) from Fitzgerald (North Acton, MA, USA); rabbit monoclonal anti-AKT (1:1000, 4691) and phospho-p44/42 (Erk 1/2) (1:2000, 4370) from Cell Signaling Technology (Leiden, The Netherlands); mouse monoclonal anti-RAC1 (1:600, ARC03) from Cytoskeleton (Denver, CO, USA); rabbit polyclonal anti-Nanog (1:100; RCAB0002P-F) from ReproCELL (Glasgow, UK); rabbit polyclonal anti-Pax-6 (1:100; PRB-278P) from Covance (Princeton, NJ, USA); chicken polyclonal anti-Neurofilament M (1:1000; 822701) from BioLegend (San Diego, CA, USA); rabbit polyclonal anti-ARHGEF6 (1:1000; A302-558A) from Bethyl Laboratories (Montgomery, TX, USA). Secondary antibodies conjugated to fluorochromes (used at 1:600 dilution) or HRP (used at 1:5000 dilution) were from Invitrogen (Carlsbad, CA, USA), Fitzgerald, SouthernBiotech (Birmingham, AL, USA) or Jackson ImmunoResearch (Cambridgeshire, UK).

Plasmids

Plasmids encoding HA-tagged RAB7^{WT} and the CMT2B-causing RAB7^{V162M} mutant protein have been previously described [36]. The pcDNA3-HA plasmid was constructed by inserting a DNA sequence coding for a 2xHA-tag into the KpnI restriction site of the pcDNA3.1 (Invitrogen, V79020) and it was used as empty vector in control transfections.

Induced pluripotent stem cells generation

iPSCs were generated reprogramming fibroblasts from healthy controls and CMT2B patients carrying the RAB7^{V162M} mutation by Sendai viral transduction of the transcription factors OCT4, SOX2, KLF4, and c-MYC (CytoTune2.0-iPS Sendai Reprogramming Kit, Thermo Fisher, Waltham, MA, USA). iPSCs were then tested for Sendai virus clearance (CytoTune2.0-iPS Sendai Reprogramming Kit, Thermo Fisher) and pluripotency (Trilineage differentiation Kit, Stem Cell Technologies, Vancouver, Canada). Cells were regularly screened and confirmed negative for mycoplasma during both maintenance and differentiation (MycAlert kit, Lonza, Basel, Switzerland).

Induced pluripotent stem cells maintenance and differentiation in dorsal root ganglia (DRG) sensory neurons

iPSCs were maintained in feeder-free conditions using mTeSR1 medium (Stem Cell Technologies) on hES qualified Matrigel (Corning, Corning, NY, USA) coated plates. At 80–90% of confluency, iPSCs were passaged using 0.5 mM EDTA in PBS (Sigma-Aldrich) or ReLeSR (Stem Cell Technologies), in the presence of ROCK inhibitor (Stem Cell Technologies). Prior to differentiation, iPSCs were

single cell dissociated with Accumax (Sigma-Aldrich) and plated onto hES qualified Matrigel coated six-well plates in the presence of ROCK inhibitor. Cells were grown in mTeSR1 medium for 24 h, then shifted to MEF-CM (Mouse embryo fibroblasts-conditioned medium) produced according to Lee et al. [44], supplemented with 10 ng/ml bFGF (Thermo Fisher). At approximately 40–50% of confluency (usually 24/48 h after the shift to CM medium), differentiation was started [45, 46]. The medium was replaced with KSR medium high glucose DMEM (Thermo Fisher) supplemented with 15% KSR (KO serum replacement, Thermo Fisher), 1 × L-glutamine (Thermo Fisher), 1 × Pen/Strep (Thermo Fisher), 1 × sodium pyruvate (Thermo Fisher), non-essential amino acids (Thermo Fisher), and 100 μM 2-mercaptoethanol (Thermo Fisher). Smad inhibitors 10 μM SB431542 (Tocris, Bristol, UK) + 0.1 μM LDN193189 (Stemgent, Cambridge, MA, USA) were added to the medium from day #0 to day #5 (see Supplemental Table 1). Three more small molecules 3 μM CHIR99021 (Tocris), 10 μM DAPT 10 μM (Tocris), and 10 μM SU5402 (Tocris) were added from day #2 to day #12. If overconfluent, cultures were split on day #2/day #3 to guarantee optimal differentiation [46]. From day #5 to day #12, the KSR medium was gradually transitioned to N2B27 medium (Neurobasal, Thermo Fisher) and added with 1% N₂ supplement (Thermo Fisher), 1% B27 supplement (Thermo Fisher), 1 × glutamine (Thermo Fisher), and 1 × pen strep (Thermo Fisher). On day #11, young neurons were detached with TrypLE Express (Thermo Fisher) and replated on GFR (growth factor reduced) Matrigel (Corning)-coated coverslips. On day #13, the cultures were shifted to neural differentiation medium (Neurobasal, Thermo Fisher), supplemented with 1% N₂ supplement (Thermo Fisher), 1% B27 (Thermo Fisher), 1% Pen-Strep (Thermo Fisher), 1% L-glutamine (Thermo Fisher), 25 ng/ml GDNF (Peprotech, London, UK), 25 ng/ml BDNF (Peprotech), 25 ng/ml NGF (Peprotech), 25 ng/ml NT3 (Peprotech), and 1 μM laminin (Sigma-Aldrich). CHIR99021 was added to neural differentiation medium for 3 days (from day #13 to day #15). 1 μM AraC (Sigma-Aldrich) was included in differentiation medium for 1 week (from day #13 to day #20) to kill off dividing cells. The treatment with AraC was repeated, if necessary, every other week (up to 3 cycles). Differentiation was usually extended from 2 to 4 weeks.

Transfection and RNA interference

Transfection of HeLa cells was performed using Metafectene Pro from Biontex (Martinsried, Germany), as indicated by the manufacturer. After 20 h of transfection, cells were processed for DQ-BSA dequenching assay. Transfection of cells with siRNA was performed using Metafectene SI from Biontex (Martinsried, Germany) as indicated by the

manufacturer. Cells were analyzed after 5 days of transfection. Small interfering RNAs (siRNAs) were purchased from MWG-Biotech (Ebersberg, Germany).

Rab7a siRNA efficiency in silencing was reported previously [36]: sense sequence 5'-GGAUGACCUCUAGGAAGAATT-3' and antisense sequence 5'-UUCUCCUAGAGGUCAUCCTT-3'. Control RNA was used as a negative control: sense sequence 5'-ACUUCGAGCGUGCAUGGCUTT-3' and antisense sequence 5'-AGCCAUGCACGCUCGAAGUTT-3'.

EGF internalization and EGFR degradation assays

For the EGF internalization assay, control and CMT2B skin fibroblasts were incubated overnight in starvation medium (0.5% BSA, 20 mM HEPES, pH 7.3, in DMEM). Cells were subsequently incubated for 1 h at 4 °C with 0.8 mg/ml rhodamine-labeled EGF (Thermo Fisher, E3481) in starvation medium and then washed several times with starvation medium. After incubation at 37 °C in complete DMEM medium for different time points (30 min, 1 h and 2 h), cells were fixed, mounted on slides, and processed for confocal microscopy. Zen 2011 software (Carl Zeiss, Oberkochen, Germany) was used for image capture and to calculate weighted colocalization coefficient of EGF and LAMP1. For EGFR degradation assay, control and CMT2B skin fibroblasts were incubated for 1 h at 37 °C with serum- and antibiotic-free DMEM and 10 µg/ml cycloheximide, then stimulated with EGF (50 ng/ml) for different times (15, 60, 180, 360 min) and lysed with RIPA buffer (50 mM Tris-HCl, pH 8.0, with 150 mM sodium chloride, 1.0% Igepal CA-630 (NP-40), 0.5% sodium deoxycholate, and 0.1% sodium dodecyl sulfate) plus protease inhibitor cocktail (Roche, Mannheim, Germany). The levels of degraded EGFR were determined by western blotting. When indicated, 100 µM chloroquine was added to the cells 3 h before harvesting.

Analysis of cathepsin D synthesis

Cells were treated with 10 µg/ml cycloheximide (to inhibit protein synthesis) for 50 h, lysed with 2×Laemmli buffer supplemented with DTT (dithiothreitol) and subjected to western blot analysis. Bands were quantified by densitometry using ImageJ software (National Institutes of Health).

Cathepsin activity assays

Cathepsin D Activity Fluorometric Assay (K143-100, BioVision, Milpitas, CA, USA) utilizes the cathepsin-D substrate sequence GKPILFFRLK(Dnp)-D-R-NH₂ labeled with fluorescent MCA (7-methoxycoumarin-4-acetic acid). 2×10⁴ control and CMT2B cells were collected and read in a fluorometer equipped with a 328-nm excitation filter and

460-nm emission filter. Cathepsin D activity was expressed by relative fluorescence units (RFU) per million cells and by RFU fold increase of CMT2B fibroblasts against control fibroblasts. Cathepsin B and Cathepsin L Activity Assay Kits (BioVision, K140-100 e K142-100) utilize, respectively, the preferred cathepsin-B RR and cathepsin-L FR substrate sequence labeled with fluorescent AFC (7-amino-4-trifluoromethylcoumarin). 2×10⁴ control and CMT2B fibroblasts were collected and read in a fluorometer equipped with a 400-nm excitation filter and 505-nm emission filter. Fold-increase in cathepsin-B or cathepsin-L activity was determined by comparing the relative fluorescence units (RFU) measured in CMT2B and control fibroblasts.

DQ-BSA dequenching assay

Cells were grown on glass coverslips and treated with DQ-BSA. Fibroblasts were treated with DQ Red BSA (10 µg/ml, Thermo Fisher, D12051) for 48 h, neurons with DQ Green BSA (50 µg/ml, Thermo Fisher, D12050) for 24 h and HeLa cells with DQ Green BSA (10 µg/ml) for 6 h. Fluorescence was quantified with Zeiss LSM 700 confocal microscope.

Western blotting

Control and CMT2B fibroblasts and neurons were lysed with Laemmli buffer [100 mM Tris-HCl, pH 6.8, 4% (w/v) SDS, 0.2% (w/v) bromophenol blue, 20% glycerol and 200 mM DTT (dithiothreitol)]. Lysates were loaded on SDS-PAGE and separated proteins were transferred onto PVDF membrane (Merck Millipore). The filter was blocked in 5% milk in PBS for 30 min at room temperature, incubated with the appropriate primary antibody and then with a secondary antibody conjugated with HRP (diluted 1:5000). When phosphorylation was monitored, cells were lysed in the presence of phosphatase inhibitors (PhosSTOP, Roche). Bands were visualized using Western blot Luminol Reagent (Santa Cruz) or Western Bright ECL kit (Advansta, Menlo Park, CA, USA) or ClarityMax (Bio-Rad). The signal was captured on a film, avoiding saturation, to ideally compare samples in the linear range of detection. To prevent saturation of the signal, we previously estimated proper loading amounts. To reduce variability, we did not quantify signals that decayed too quickly and we avoided comparing very weak bands that may be outside the linear range. Films were then scanned at 600 dpi resolution and quantified using ImageJ (National Institutes of Health). Each band was quantified selecting rectangular areas and subtracting the film background. Bands relative to the protein of interest and to the related tubulin loading control were quantified. Measurement of each protein was then normalized on the related tubulin loading control and CMT2B normalized measurements were compared

to control normalized measurements obtained from the same gel.

Confocal immunofluorescence microscopy

Fibroblasts grown on coverslips were permeabilized, fixed and incubated with primary and secondary antibodies as described previously [47] and viewed with Zeiss LSM 700 confocal microscope. HeLa cells were fixed for 20 min in 3% paraformaldehyde, permeabilized with 0.1% TX100 in PBS and then incubated with primary and secondary antibodies diluted in 0.1% saponin in PBS. Then, washing, cells were stained with DAPI and coverslips were mounted and viewed with Zeiss LSM 700 confocal microscope.

iPS cells or peripheral neurons were fixed for 20 min in 4% paraformaldehyde, blocked and permeabilized for 20 min with 10% NGS, 1% BSA, and 0.1% TX100. Alternatively, cells were fixed and permeabilized for 10 min in ice-cold methanol at -20°C . After incubation with primary antibody overnight at 4°C , the coverslips were washed, incubated with the secondary antibody for 30 min, washed, and mounted with DAPI (H-1200, Vector Laboratories, Burlingame, CA, USA) and viewed with Leica SP5 confocal microscope.

Electron microscopy

Cells were fixed in 2% glutaraldehyde in 0.2 M Hepes, pH 7.4, at room temperature for 2 h. During fixation, the cells were scraped off the culture dish and pelleted. After post-fixation in 1% osmium tetroxide, cells were dehydrated in ethanol and embedded in epoxy resin. Sections were cut with a diamond knife and contrasted with uranyl acetate and lead citrate. Microscopy was performed with a Jeol JEM 1400 Plus transmission electron microscope.

Real-time PCR

For RT-PCR on fibroblasts, RNA was isolated from cells using an RNeasy Micro kit according to the manufacturer's instructions (Qiagen, Hilden, Germany). For RNA retrotranscription protocol, we used SuperScript II Reverse Transcriptase (Invitrogen) according to the manufacturer's instructions. Briefly, a mixture (12 μl) containing 4 μg of RNA, 10 mM of deoxynucleotides and 40 ng of random primers (Promega, Madison, WI, USA) was heated at 65°C for 5 min. First-strand cDNA synthesis was carried out with SuperScript II Reverse Transcriptase in the presence of dithiothreitol (0.01 M) and ribonuclease inhibitor (40 U, RNaseOUT, Invitrogen) at 42°C for 50 min. Reactions were stopped by heat inactivation at 70°C for 15 min.

Quantitative real-time PCR was carried out with Power SYBR Green (Applied Biosystems, Foster City, USA) using Applied Biosystems 7900HT Fast Real-time PCR System.

The primers used were:

GAPDH: *forward*: 5'-GGTGGTCTCCTCTGACTTCAACA-3',

reverse: 5'-GTTGCTGTAGCCAAATTCGTTGT-3'.

Cathepsin B: *forward*: 5'-CTGTCCGATGAGCTGGTCAAC-3',

reverse: 5'-TCGGTAAACATAACTCTCTGGGG-3'.

Cathepsin D: *forward*: 5'-CAGAAGCTGGTGGACCAGAAC-3',

reverse: 5'-TGCGGGTGACATTCAGGTAG-3'.

Cathepsin L: *forward*: 5'-GCTAATGACACCGGCTTTGT-3',

reverse: 5'-TTTCAAATCCGTAGCCAACC-3'.

LAMP1: *forward*: 5'-ACGTTACAGCGTCCAGCTCAT-3',

reverse: 5'-TCTTTGGAGCTCGCATTGG-3'.

LAMP2: *forward*: 5'-TGCTGGCTACCATGGGGCTG-3',

reverse: 5'-GCAGCTGCCTGTGGAGTGAGT-3'.

These were purchased from Eurofins Genomics (Ebersberg, Germany).

The thermal profile used for Real-time PCR was as follows: 1 cycle of 2 min at 50°C ; 1 cycle of 10 min at 95°C ; 40 cycles of 15 s at 95°C , 1 min at 55°C ; 1 cycle of 15 s at 95°C and 15 s at 60°C . The specificity of PCR products was checked by performing a melting-curve test. The relative expression level was calculated using the comparative C_T method and expressed as a "fold change". The quantitative values were obtained from the mean minimal cycle threshold (C_T) calculated from triplicate reactions. The fold change, measured as the amount of target gene normalized to the endogenous reference gene GAPDH, was given by $2^{-\Delta\Delta C_T}$, where $\Delta C = C_{T\text{target}} - C_{T\text{GAPDH}}$ and $\Delta\Delta C_T = \Delta C_{T\text{sample}} - \Delta C_{T\text{control}}$. Negative fold change was calculated using the formula $-1/2^{-\Delta\Delta C_T}$. The relative quantification was considered significant when there was a minimum of twofold change.

For RT-PCR on iPS or iPS-derived cells, in brief, iPS cell clones and differentiated iPSCs tested for pluripotency (Tri-lineage differentiation Kit, Stem Cell Technologies) were homogenized with TRIzol reagent (15596026; Invitrogen) and total RNA was extracted with chloroform and precipitated with isopropanol. A portion (500 ng) of total RNA was reverse transcribed using High-Capacity cDNA Reverse Transcription Kits (4368814, Applied Biosystems), according to the manufacturer's instructions. Semiquantitative RT-PCR analyses were performed with GoTaq G2 Flexi DNA Polymerase (M7805, Promega). Primer sequences are shown in Supplemental Table 2, while primers used to test iPSCs

for Sendai virus clearance derived from CytoTune2.0-iPS Sendai Reprogramming Kit (Thermo Fisher).

Wound-healing assay

Confluent monolayer of fibroblasts was wounded with a pipette tip. The cell debris was washed out with PBS. Cells were imaged at the moment of the scratch (T0) and after 15 h using a 10× objective of EVOS digital microscope. Accumulated distance was measured using photoshop software as the total distance that cells traveled in a certain amount of time.

Gelatin zymography

The conditioned medium was collected from cells cultured for 24 h in serum-free medium, the sample was concentrated using Amicon® Ultra (Merck Millipore) and quantified by Bradford assay. Each sample was adjusted to 15 µg/ml, and 10 µl was loaded in non-reduced protein sample buffer on 7.5% SDS-PAGE gel containing 1 mg/ml gelatin (Biorad). The gel was washed in a specific buffer (2.5% Triton X-100, 50 mM Tris-HCl pH 7.5, 5 mM CaCl₂, 1 µM ZnCl₂) to remove SDS and then three times in distilled water. After washing, the gel was incubated at 37 °C for 24 h in a buffer containing 1% Triton X-100, 50 mM Tris-HCl pH 7.5, 5 mM CaCl₂, 1 µM ZnCl₂ and then was stained with 0.5% Coomassie Blue R-250 (Sigma-Aldrich) and destained in 40% methanol and 10% acetic acid.

Rac1 activity assay

Rac1 activity was tested following the manufacturer's protocol with Rac1 Pull-down Activation Assay Biochem Kit (BK035, Cytoskeleton). Briefly, lysates were mixed with GST-Pak-PBD beads for 1 h at 4 °C. After washing, the pelleted beads were resuspended in Laemmli sample buffer and subjected to SDS-polyacrylamide gel electrophoresis. GTP-bound Rac1 was detected by western blot analysis using anti-Rac1 antibody. The total amount of Rac1 was detected by immunoblotting of the whole cell lysates.

Teratoma formation

iPSCs were preincubated with mTeSR1 (Stem Cell Technologies), added with ROCK inhibitor (Stem Cell Technologies) for 1 h, harvested by Accumax (Sigma-Aldrich) treatment, collected into tubes, and centrifuged, and the pellets were suspended in PBS 1× (Sigma-Aldrich) with ROCK inhibitor. One-third of the cells from a confluent 35 mm dish was injected in the testis of 8 weeks old Fox Chase SCID Beige mice (Strain Code: 250, Charles River). Six weeks after injection, tumors were dissected and fixed with

formaldehyde solution. Paraffin-embedded tissue was sliced and stained with hematoxylin and eosin. All animal experiments were approved and performed in compliance with the guidelines of San Raffaele Institutional Animal Care and Use Committee.

DNA sequence analysis of RAB7

Genomic DNA was extracted from pelleted neurons using GenElute Mammalian Genomic DNA Miniprep Kit (Sigma-Aldrich) according to the manufacturer's protocol. 100 ng of genomic DNA was amplified by PCR using the following primers for exon 4: 5' CTGTGTCCTCACCTGTACTACC 3' and 5' GAAAAGAGTGGGTTAGGGAAGAAG 3'. PCR conditions for this reaction are: 94 °C for 7 min, (94 °C for 1 min, 55 °C for 30 s, 72 °C for 45 s) × 30 cycles followed by a final step at 72 °C for 7 min. PCR products were loaded on agarose gel and extracted using QIAEX II Gel Extraction Kit (Qiagen, Hilden, Germany). Samples were shipped to Eurofins Genomics (Ebersberg, Germany) for sequencing.

Neurite length analysis

Neurite length was measured by IncuCyte® S3 Live-Cell Analysis System (Essen BioScience). Briefly, young neurons were plated in 24-well plate (20,000 cells/well). Bright field (contrast) real-time automated acquisition and measurements for live cells were performed every 4 h for the first six consecutively days after neuron plating. Two wells per clones were plated and sixteen field per well were analyzed (objective 20×). Neurite length was measured as detected by the IncuCyte Zoom software as the total combined length of all neurites (mm) detected per mm². All data are expressed relative to the respective day 0 of maturation. Each group is represented by mean ± SEM ($n = 32$).

Statistical analysis

Data were statistically analyzed using Student's *t* test and Mann-Whitney *U*-test (GraphPad Prism4 software) (* $p < 0.05$, ** $p < 0.01$ and $p < 0.001$). Error bars represent SEM. Experiments were performed at least in triplicate.

Results

Late endocytic protein expression is altered in CMT2B fibroblasts

To investigate possible endocytic and lysosomal defects in CMT2B, we used previously isolated dermal fibroblasts from a CMT2B patient carrying the RAB7^{V162M} mutation and from a healthy age- and sex-matched control [43].

We analyzed first the expression of early endocytic RABs and found comparable amounts of RAB5, a protein controlling early endosomal homotypic fusion and transport from plasma membrane to early endosome [47, 48], as well as of RAB4, a protein regulating different steps of endocytic recycling [49] (Fig. 1a). Next, we looked at late endocytic RAB proteins, such as RAB7 and RAB9, whose abundance increases during early to late endosome transition [1, 50]. Similar amounts of RAB7, which is mutated in CMT2B neuropathy, were found in CMT2B compared to control fibroblasts (Fig. 1a). However, we observed a strong increase in the levels of RAB9 (Fig. 1a) of about twofold in

CMT2B compared to control cells. Subsequently, we investigated the abundance of other late endosomal and lysosomal markers such as lysosomal associated membrane protein 1 and 2 (LAMP1 and LAMP2) [1, 51] in fibroblasts derived from three CMT2B patients of the same Italian family [33] and from two healthy individuals. We observed that, compared to the controls, all CMT2B patients showed higher abundance of LAMP1 and LAMP2, although to a different extent (Fig. 1b, c). We then silenced RAB7 in CMT2B fibroblasts and observed reduced abundance of LAMP1, thus suggesting that the different expression of LAMP proteins in CMT2B cells is most likely related to RAB7 (Fig. 1d).

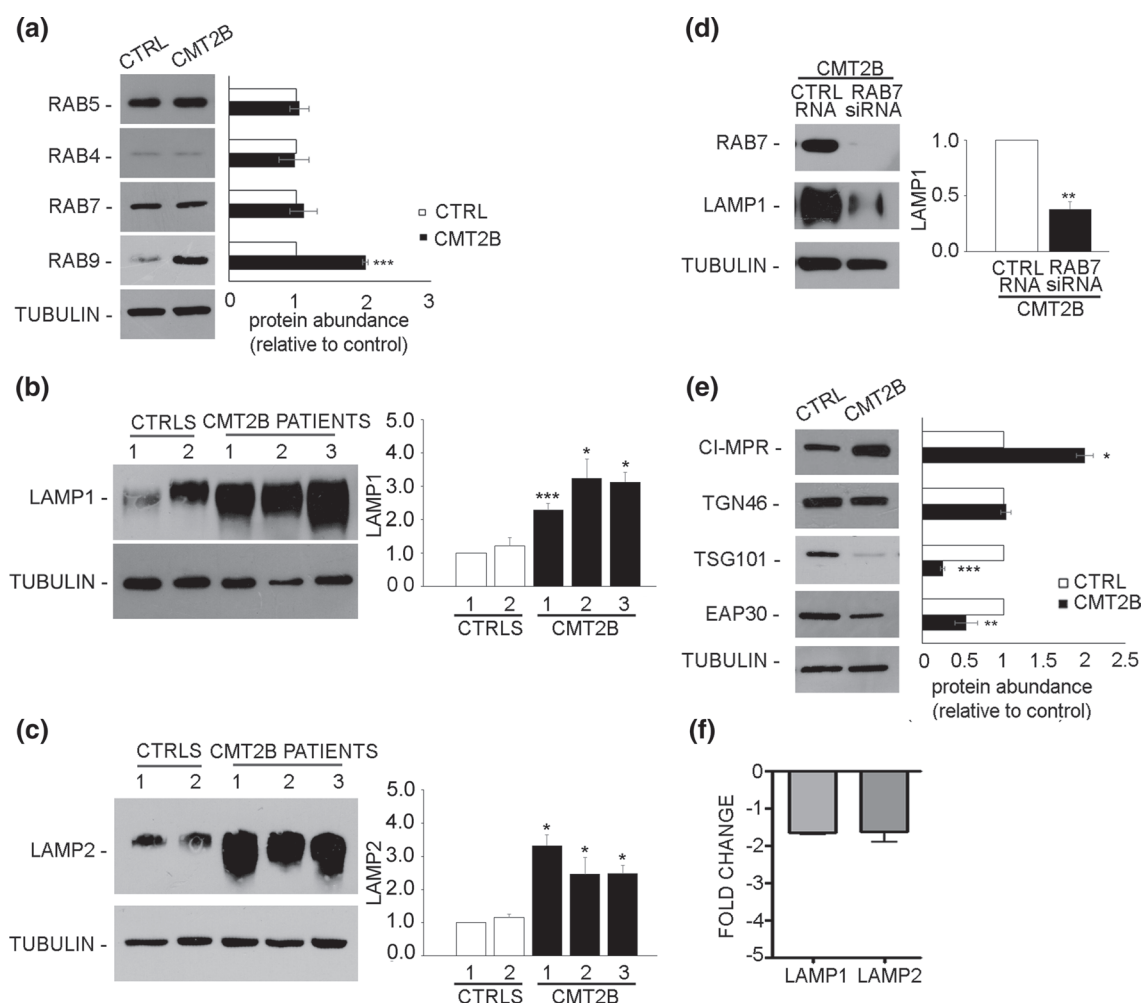


Fig. 1 Analysis of endosomal and lysosomal markers in control and CMT2B fibroblasts. **a** Lysates of control and CMT2B patient 1-derived skin fibroblasts carrying the RAB7^{V162M} mutation were analyzed by immunoblotting using anti-RAB5, anti-RAB4, anti-RAB7 and anti-RAB9. **b, c** Lysates of two controls and three CMT2B skin fibroblasts carrying the RAB7^{V162M} mutation were analyzed by immunoblotting using anti-LAMP1 (**b**) and anti-LAMP2 (**c**) antibodies. **d** CMT2B fibroblasts were silenced for RAB7 and then LAMP1 abundance was analyzed by immunoblotting using anti-LAMP1 antibody. **e** Lysates of control and CMT2B patient 1-derived skin

fibroblasts were analyzed by immunoblotting using anti-CI-MPR, anti-TGN46, anti-TSG101 and anti-EAP30 antibodies. Bands were quantified using NIH ImageJ and normalized against tubulin. **f** The amount of LAMP1 and LAMP2 transcripts was quantified, compared to the GAPDH transcript as control, using real-time PCR in control and CMT2B patients-derived fibroblasts. All data represent the mean \pm SEM of at least three experiments. Statistical analysis was performed using Student's *t* test with control fibroblasts as referring sample. **p* < 0.05; ***p* < 0.01; ****p* < 0.001

We then looked at the expression of cation independent mannose-6-phosphate receptor (CI-MPR), a protein involved in transport between Golgi and endosomes, and TGN46, localized to the trans-Golgi network [51–53]. We found that, in CMT2B fibroblasts, the expression of CI-MPR was two-fold higher than in control cells (Fig. 1e), while the expression of TGN46 did not change (Fig. 1e).

Sorting events play a crucial role in endocytosis and control correct cargo shipment to lysosomes. Among proteins important for sorting at the level of early endosomes, endosomal sorting complex required for transport (ESCRT) proteins are fundamental for targeting signaling receptors to degradation [54]. Therefore, we decided to investigate the abundance of some of these proteins in CMT2B cells. We found that tumor susceptibility gene 101 (TSG101) was strongly decreased in CMT2B fibroblasts compared to control cells (Fig. 1e), while the expression of ELL (eleven-nineteen lysine-rich leukemia) associated protein 30 (EAP30), the homolog of yeast VPS22, was about 40% lower in CMT2B fibroblasts (Fig. 1e), suggesting that ESCRT proteins are down-regulated in CMT2B.

To establish whether the observed changes in the amount of late endosomal and lysosomal markers were a consequence of mRNA abundance, we measured LAMP1 and LAMP2 mRNA expression using real-time PCR (Fig. 1f). As the relative quantification is considered significant when there is minimum of twofold change, the mRNA levels of LAMP1 and LAMP2 were not significantly changed (Fig. 1f).

Altogether, these results indicate that in CMT2B fibroblasts, the abundance of early endocytic markers is not affected, the expression of sorting proteins regulating the lysosomal biogenesis is reduced, while the expression of lysosomal protein is increased, suggesting that the late endocytic pathway is altered and that these changes are due to modified RAB7 activity.

CMT2B cells have more lysosomes

We next investigated the abundance of lysosomes in CMT2B cells by immunofluorescence analysis. In control cells, using antibodies against LAMP1, a marker of late endosome and lysosomes, we observed, as expected the presence of many LAMP1-positive organelles mostly concentrated around the nucleus (Fig. 2a). Staining of CMT2B cells revealed a similar distribution, but a stronger staining of these structures present in the perinuclear area (Fig. 2a), as confirmed by quantification (Fig. 2a).

Immunoblotting (Fig. 1b, c) and immunofluorescence data (Fig. 2a) suggest that the amount of lysosomes may be increased in patient cells. To investigate this, we performed electron microscopy, demonstrating that patient cells were actually filled with lysosomes (Fig. 2b). Quantification of the

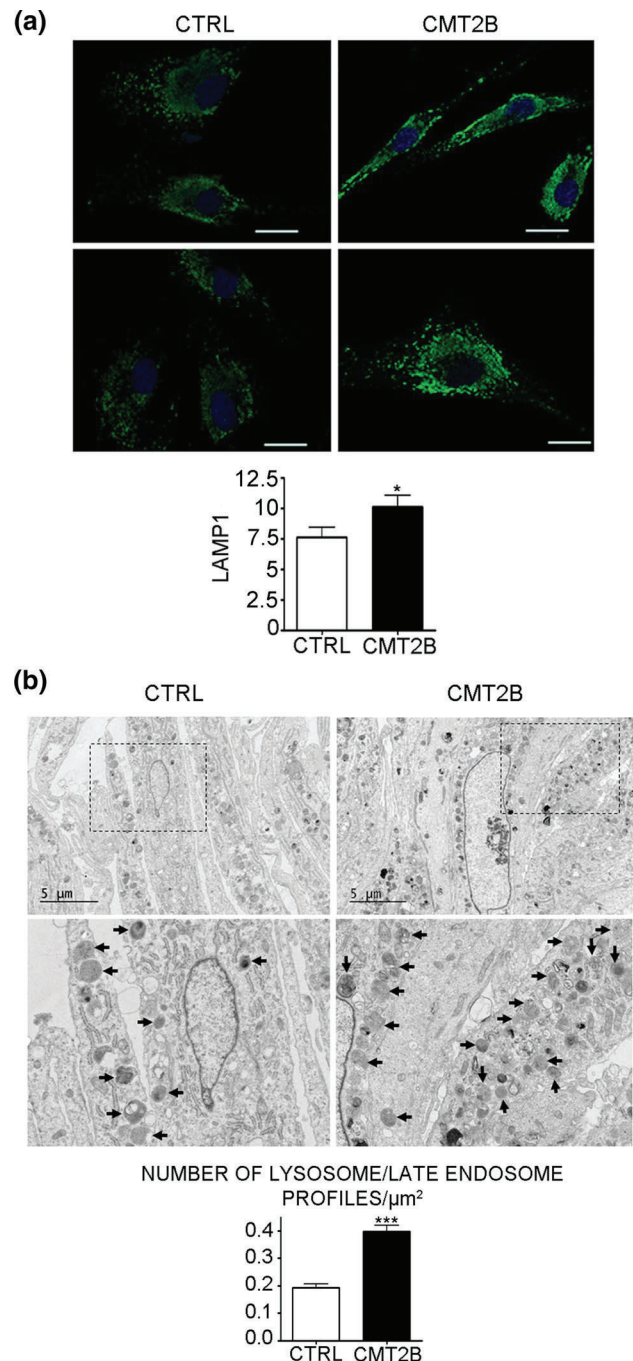


Fig. 2 Electron microscopy of control and CMT2B patient 1 fibroblasts. **a** Control and CMT2B fibroblasts from patient 1 carrying the RAB7^{V162M} mutation were fixed and immunolabeled with anti-LAMP1 followed by Alexa488-conjugated secondary antibody, while nuclei were stained with DAPI. Bars 20 μm . LAMP1 intensities of at least 50 cells per sample were measured using ImageJ. Graphs were generated with GraphPad. Mann–Whitney *U* test was used for statistical analysis and control fibroblasts were selected as referring sample. **p* < 0.05. **b** The boxed areas are shown at higher magnification in the lower panels. Arrows indicate some of the lysosomes. Bars 5 μm . Graphs of lysosome number quantification were generated with GraphPad. Mann–Whitney *U* test used for statistical analysis and control fibroblasts were selected as referring sample. ****p* < 0.001

number of lysosome profiles in thin sections demonstrated that CMT2B cells have about twice as many lysosomes as compared to control cells (Fig. 2b), while no alterations in the formation of multivesicular bodies were observed (Fig. 3).

Altogether, these data indicate that CMT2B cells have more lysosomes.

CMT2B fibroblasts show higher lysosomal activity

The higher abundance of late endocytic proteins and of lysosomes in CMT2B cells prompted us to hypothesize a higher lysosomal activity in CMT2B fibroblasts. Cathepsin-D is a lysosomal enzyme synthesized as an inactive precursor (pre-pro-cathepsin), converted into pro-cathepsin D (52 kDa) in the endoplasmic reticulum and further processed into late endosomes and lysosomes into the 44-kDa form and then into the 32-kDa mature form [55–57]. Defects in cathepsin-D maturation correlate with alterations of lysosomal functions. Using a specific antibody able to detect the different immature and mature forms of cathepsin D, we could detect the immature forms both in control and CMT2B fibroblasts (Fig. 4a). Quantification of the ratio of immature cathepsin D on total cathepsin D indicates that cathepsin D

processing is more efficient in CMT2B cells (Fig. 4a). In addition, quantitative analysis of the total amount of mature cathepsin D revealed that cathepsin D abundance in CMT2B fibroblasts was about twofold higher than in control cells (Fig. 4a). Treatment with cycloheximide, an inhibitor of protein synthesis, lowered this increase, suggesting that the higher amount of cathepsin D is due to increased protein synthesis (Fig. 4b).

Cathepsin D is important not only for lysosomal activity, but also for lysosome-mediated apoptosis [55]. To understand whether cathepsin D increase in CMT2B cells correlates with higher degradation activity, we performed a cathepsin D activity assay based on fluorescence release upon cleavage of a substrate. CMT2B fibroblasts showed higher fluorescence (Fig. 4c) and quantification revealed that cathepsin D activity in CMT2B cells was approximately 40% higher than in control fibroblasts (Fig. 4d).

To confirm increased lysosomal activity, we decided to test the enzymatic activity of other lysosomal proteins such as cathepsin-L and cathepsin-B using similar fluorescence-based assays on patient 1 fibroblasts. Both cathepsin L and cathepsin B activities were about 40% higher in CMT2B cells compared to control cells (Fig. 4e, f), thus confirming increased lysosomal activity. To establish whether the higher

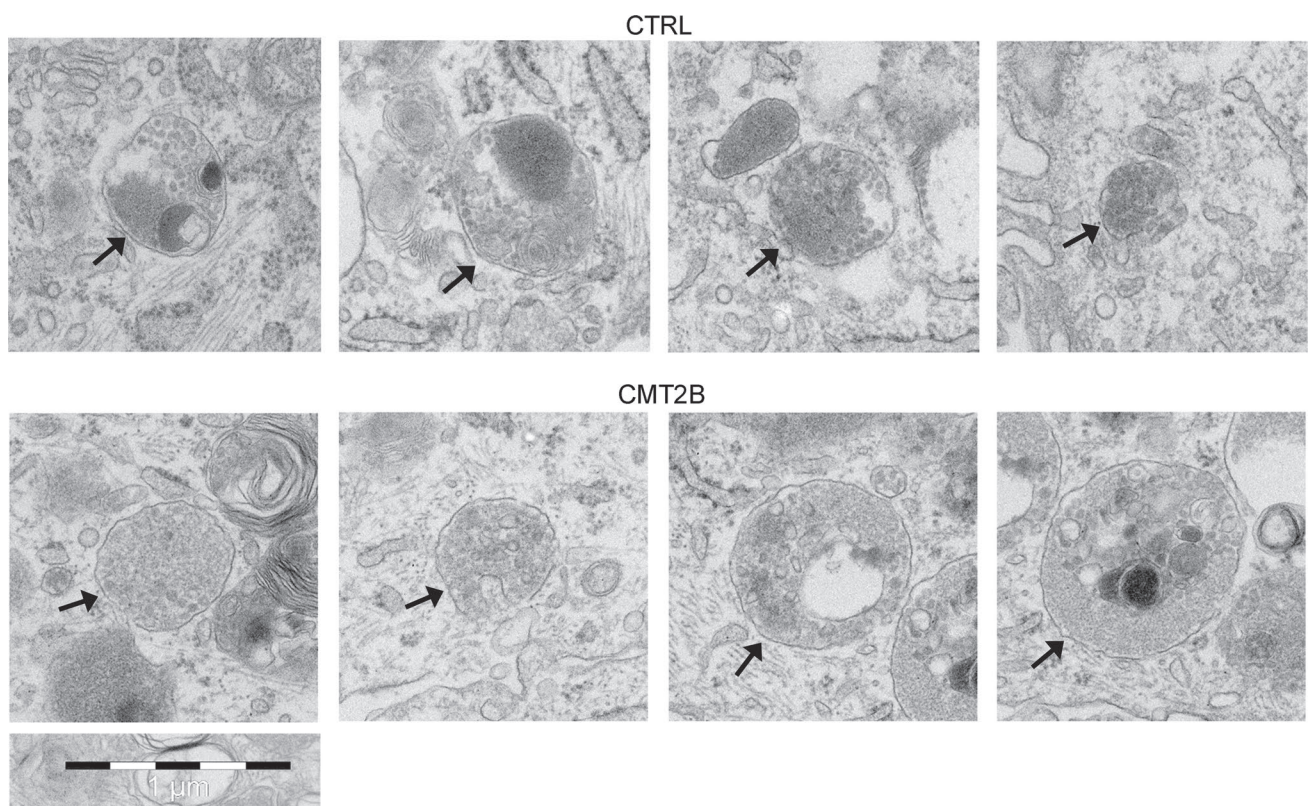
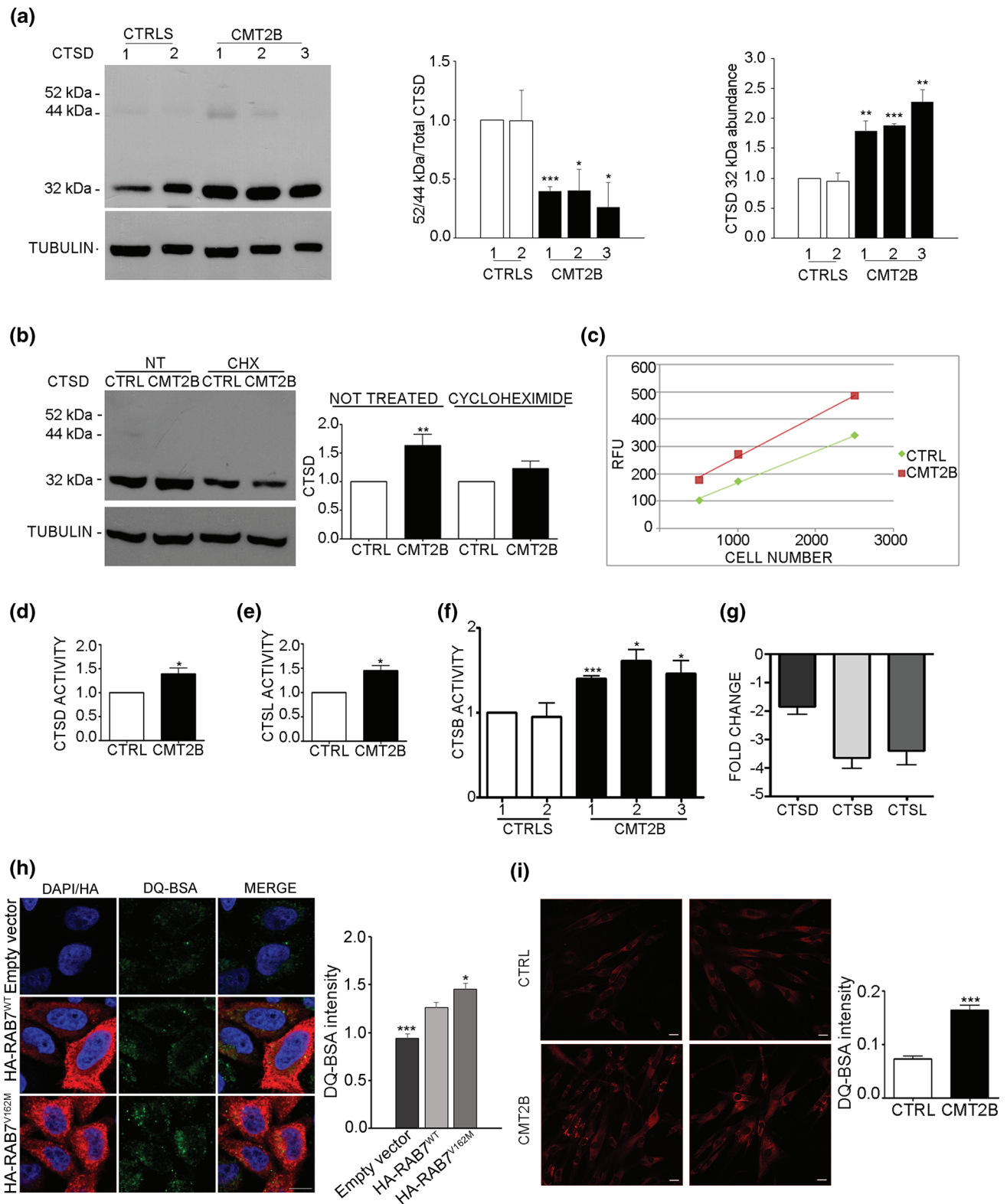


Fig. 3 Electron microscopy of multivesicular bodies from control and CMT2B patient 1 fibroblasts. Arrows indicate multivesicular bodies (MVBs) observed in control and CMT2B patient 1 carrying the RAB7^{V162M} mutation. Bar 1 μm



activity of cathepsins observed was a consequence of alterations in gene expression, we analyzed mRNA abundance and measured cathepsin B, D and L mRNA expression using real-time PCR (Fig. 4f). The mRNA levels of cathepsin D

were not significantly changed, while cathepsin B and L mRNAs were decreased, possibly due to a compensatory mechanism to counteract the higher amount and activity of these proteins (Fig. 4g).

Fig. 4 Lysosomal activity in CMT2B fibroblasts carrying the RAB7^{V162M} mutation. **a** Lysates of two controls and CMT2B fibroblasts from three patients were subjected to immunoblotting using anti cathepsin D (CTSD) and anti-tubulin antibodies. Intensities of bands were measured by densitometry and normalized against tubulin. **b** Lysates of control and CMT2B fibroblasts from patient 1 untreated or treated with cycloheximide for 50 h were subjected to immunoblotting using anti cathepsin D and anti-tubulin antibodies. Intensities of bands were measured by densitometry and normalized against tubulin. **c** Different dilutions of control and CMT2B patient 1 lysates were tested for ability to cleave the MCA-labeled synthetic substrate. RFU per each dilution was evaluated after fluorimetric analysis. **d** Quantification of fluorescence data to evaluate cathepsin-D activity in control and CMT2B fibroblasts (patient 1). **e** The ability of cathepsin-L (CTSL) to cleave the substrate was evaluated in both control and CMT2B patient 1-derived fibroblasts. **f** Fibroblasts derived from two distinct control individuals and three CMT2B patients were analyzed to test cathepsin B (CTSB) activity. **g** The amount of cathepsin-D, L and B transcripts was quantified, compared to the GAPDH transcript as control, using real-time PCR, in control and CMT2B patients-derived fibroblasts. **h** HeLa cells were transfected for 24 h with the empty vector or plasmids encoding HA-tagged RAB7^{WT} or CMT2B-causing mutant RAB7^{V162M}. Cells were incubated for 6 h with DQ Green BSA and then processed for immunofluorescence analysis. Bar 10 μm . DQ BSA intensities were measured using ImageJ and Corrected Total Cell Fluorescence (CTCF) was calculated. Data represent the mean \pm SEM of at least 50 cells analyzed. Student's *t* test was used for statistical analysis. Statistical comparisons of the samples are with RAB7^{WT}. **p* < 0.05; ****p* < 0.001. **i** Control and CMT2B fibroblasts from patient 1 were treated with DQ-BSA for 48 h, then fixed and observed on a confocal microscope. Bars 20 μm . The intensities of manually determined areas for each single cell were measured using Image J. At least 50 cells per sample were analyzed. Graphs were generated with Graph-Pad. All data represent the mean \pm SEM of at least three independent experiments. Student's *t* test or Mann–Whitney *U* test (for DQ-BSA quantification) was used for statistical analysis and control fibroblasts were selected as referring sample. **p* < 0.05; ***p* < 0.01, ****p* < 0.001

To further investigate lysosomal activity, we used the DQTM BSA assay in which cells are incubated with the self-quenched DQTM BSA, whose cleavage by proteases in an acidic compartment generates a highly fluorescent product. HeLa cells transfected with the empty vector or with a construct encoding HA-tagged RAB7^{WT} or the CMT2B-causing mutant RAB7^{V162M} were incubated with DQ-BSA. After 6 h of incubation with DQTM Green BSA, HeLa cells expressing CMT2B-causing mutant RAB7^{V162M} showed higher fluorescence compared to cells transfected with empty vector and plasmid encoding HA-tagged RAB7^{WT} (Fig. 4h). Similarly, control fibroblasts and CMT2B fibroblasts from patient 1 were analyzed after 48 h of incubation with DQTM Red BSA. Control fibroblasts displayed a lower level of fluorescence compared to CMT2B fibroblasts and quantification revealed an approximately two-fold increase of fluorescence in CMT2B compared to control cells (*p* < 0.0001) (Fig. 4i).

Altogether, these data demonstrate that lysosomal activity in CMT2B cells is higher than in control cells and that this is caused by the expression of the RAB7^{V162M} mutant protein.

EGFR degradation is higher in CMT2B cells

The higher expression of late endocytic proteins, the lower abundance of sorting regulators and the increased number of lysosomes and lysosomal activity suggest alterations of the degradative pathway in CMT2B fibroblasts. RAB7 regulates trafficking and degradation of EGFR and previous data on EGFR degradation obtained on cells transiently or stably transfected with the CMT2B-causing RAB7 mutant proteins produced conflicting results. In fact, transient expression of CMT2B-causing RAB7 mutant proteins in HeLa cells caused normal or increased EGFR degradation [35, 36], while in HeLa and PC12 stable cell lines expressing these mutant proteins inhibition of EGFR degradation was reported [58].

To solve this issue and establish if also EGFR degradation is affected in CMT2B cells, we measured EGFR degradation in CMT2B fibroblasts carrying the RAB7^{V162M} mutation (Fig. 5a). Control and CMT2B cells were able to degrade EGFR efficiently but, notably, CMT2B fibroblasts showed a higher degradation activity at 360 min. In fact, quantification of EGFR degradation at 360 min in CMT2B patient 1 and patient 2 was significantly higher than controls, while in patient 3 was higher but not statistically significant (Fig. 5b). EGFR degradation assay at different time points on control and patient 1 fibroblasts revealed increased degradation both at time point 180 and 360 min (Fig. 5c). Our results are in agreement with previous data obtained on transiently transfected HeLa cells, but also with data on transferrin receptor degradation that was increased in fibroblasts from CMT2B patient 1 [35, 36, 43].

To evaluate if higher degradation is due to increased trafficking speed, we performed an EGF internalization assay and measured colocalization between internalized Rhodamine-EGF and LAMP1 at different time points. Interestingly, we found that in patients' fibroblasts rhodamine-EGF and LAMP1 colocalization is higher at 1 h and 2 h compared to controls indicating that trafficking to late endosomes and lysosomes is faster in CMT2B fibroblasts compared to control cells (Fig. 5d).

These results, together with quantitative analysis of late endocytic proteins, strongly indicate that the endocytic degradative pathway is increased in CMT2B fibroblasts.

EGFR signaling and cell migration are altered in CMT2B fibroblasts

The activation of EGFR stimulates a number of signaling pathways, among which are phosphatidylinositol 3 kinase (PI3K/AKT) and Ras-mitogen-activated protein kinase (MAPK) pathways, to promote cell survival and proliferation [59]. To identify downstream factors of EGFR affected in CMT2B, we analyzed the abundance and activation of